ASTRONOMY & ASTROPHYSICS
SUPPLEMENT SERIES

Astron. Astrophys. Suppl. Ser. **129,** 593-602 (1998)

BVRI surface photometry for a sample of 14 Sb galaxies⋆,⋆⋆

B. Cunow[1,2]

[1] Department of Mathematics, Applied Mathematics and Astronomy, University of South Africa, P.O. Box 392, Pretoria 0003, South Africa
e-mail: cunowbhl@risc5.unisa.ac.za or cunowbhl@alpha.unisa.ac.za
[2] Astronomisches Institut der Westfälischen Wilhelms-Universität Münster, Wilhelm-Klemm-Str. 10, 48149 Münster, Germany

Received June 10; accepted October 24, 1997

Abstract. Profiles of surface brightness, ellipticity and position angle obtained from CCD-*BVRI* images are presented for a sample of 14 spiral galaxies with $13 < B_{\rm T} < 16.1$. For these galaxies, exponential disc components were fitted to the profiles. A decrease of disc scalelengths from B to I is found for 13 galaxies, while for one galaxy scalelengths increase from B to I. The scalelength ratios $r_{\rm D}(B)/r_{\rm D}(I)$, $r_{\rm D}(V)/r_{\rm D}(I)$ and $r_{\rm D}(R)/r_{\rm D}(I)$ show a systematic increase with increasing apparent ellipticity. The maximum variation is found for $r_{\rm D}(B)/r_{\rm D}(I)$ which is 80% larger for edge-on galaxies than for face-on galaxies.

Key words: galaxies: spiral — galaxies: photometry

1. Introduction

In the last years surface brightness profiles of a number of spiral galaxies have been published. Most of the data were obtained in the optical region (e.g., Courteau 1996; Héraudeau & Simien 1996 and references therein) but with the development of infrared arrays an increasing number of galaxies was measured in the infrared bands as well (e.g., Peletier et al. 1994; Héraudeau et al. 1996). Measurements of surface brightness profiles of galaxies are essential for quantitative investigations of galaxy morphology, decomposition of bulge and disc, studies of galaxy structure and stellar populations and measurements of dust distribution. Results from these studies give important information about the distribution of the luminous mass in a galaxy. Together with dynamical information (e.g., rotation curves) this leads to results about the dark matter distribution. Other important aspects are galaxy formation and evolution.

The surface brightness profile of a galaxy is produced by the spatial distribution of the stars as well as the spatial distribution of the dust. Since the amount of dust extinction in galaxies is still an unsolved problem, the surface brightness distributions of galaxies unaffected by dust are not clearly known. One way to obtain information about the dust content in a galaxy is to study surface brightness profiles in different wavelength bands ranging from the optical to the infrared region. Since the extinction of light in the infrared K-band is negligible, K-images of galaxies are used to determine the stellar distribution. Comparison with images obtained in the optical region gives information on the dust content of the galaxy. This approach has been used by various authors (e.g., Peletier et al. 1994; Block et al. 1994a,b). Byun et al. (1994) have shown from model calculations that the differences in dust extinction between the B- and I-bands are large enough for $B-I$ colour profiles being a proper diagnostics for measuring the dust content of spiral galaxies.

A very important parameter for the stellar distribution within a spiral galaxy is the scalelength of the disc. However, scalelengths are also affected by the distribution of the dust. Measurements have shown that disc scalelengths of spiral galaxies tend to vary systematically with wavelength (see, e.g., Elmegreen & Elmegreen 1984; Peletier et al. 1994; Evans 1994). The shorter the wavelength, the larger is the disc scalelength. This means that significant colour gradients are present in discs of spirals. It is not clear yet to which extent these gradients are caused by gradients in the stellar population, by metallicity gradients or by dust extinction (Peletier et al. 1994; Evans 1994).

In this paper, profiles of surface brightness, apparent ellipticity and position angle in *BVRI* of a sample of 14 spiral galaxies are presented. For these galaxies, no *BVRI* surface brightness profiles have been published yet.

Send offprint requests to: B. Cunow

⋆ Based on observations collected at the South African Astronomical Observatory, Sutherland, Republic of South Africa.

⋆⋆ The profile data used for Figs. 1a to 1n are available in electronic form at the CDS via anonymous ftp to cdsarc.u-strasbg.fr (130.79.128.5) or via http://cdsweb.u-strasbg.fr/Abstract.html

Table 1. List of sample galaxies. All parameters are taken from the ESO-LV catalogue (Lauberts & Valentijn 1989). T denotes the morphological type, ϵ the apparent ellipticity, and PA the position angle

ESO-LV	α(1950.0)			δ(1950.0)			T	B_T	$B_T - R_T$	ϵ	PA(°)
no.	h	m	s	°	′	″					
339−0120	19	55	06	−40	57	00	4.0	13.76	1.06	0.18	0.7
463−0200 (= IC 5039)	20	40	11	−30	02	00	3.0	13.45	1.17	0.64	152.8
235−0080 (= NGC 6970)	20	48	39	−48	57	54	2.6	13.16	1.16	0.24	110.2
286−0630	21	06	32	−45	43	54	3.0	13.98	1.08	0.53	45.1
411−0170	00	45	29	−29	28	42	3.0	15.73	1.46	0.33	64.5
351−0180	00	51	25	−33	34	00	4.0	15.27	1.11	0.73	0.6
351−0220	00	52	45	−36	55	42	3.0	15.56	1.21	0.45	164.7
351−0240	00	54	50	−36	51	42	3.0	16.07	1.46	0.78	142.4
351−0250	00	56	01	−36	55	48	3.0	15.28	1.35	0.34	110.5
351−0310	00	58	39	−35	30	42	3.0	15.43	1.41	0.34	169.4
412−0210	01	12	09	−31	26	42	3.0	14.89	1.38	0.63	36.8
352−0400	01	16	44	−36	11	18	4.0	15.32	1.22	0.46	176.2
352−0540	01	19	13	−36	48	18	3.0	15.19	1.38	0.75	121.7
352−0720	01	22	56	−36	04	36	3.0	15.12	1.27	0.39	173.4

All sample galaxies are found in the ESO-LV catalogue (Lauberts & Valentijn 1989). The profiles presented in this paper will be used to study the dust content of these galaxies in detail.

An exponential disc is fitted to each profile. The comparison of the scalelengths at different wavelengths shows a systematic decrease of disc scalelength with increasing wavelength for 13 of the 14 sample galaxies and confirms the presence of large colour gradients within galaxy discs.

2. The data

2.1. Sample

The sample galaxies were chosen according to the following selection criteria: (i) morphological type $2.0 \leq T \leq 4.0$, (ii) magnitude $B_T \leq 16.1$ and (iii) colour $1.0 \leq (B_T - R_T) \leq 1.5$. Apparent ellipticities ϵ cover the whole range from face-on to edge-on view. The reason for using these criteria is to obtain a sample which is on the one hand appropriate for measurements of internal extinction and on the other hand representative for the photographic catalogue of spiral galaxies used by Cunow (1992) and Cunow & Wargau (1996) for statistical investigations of internal extinction.

The photographic catalogue is part of the Muenster Redshift Project MRSP (Schuecker et al. 1996a,b), which uses filmcopies of the ESO/SERC J- and R-surveys and low-dispersion objective prism plates. The internal extinction was measured for a magnitude-limited sample of spiral galaxies in the ESO/SERC field Nos. 351, 352, 411 and 412. In addition to J- and R-data, U- and I-plates of these fields were also used.

In order to allow comparison, the galaxies used in this work were selected to be members of the photographic sample. This restricts the magnitude range to $14 < B_T < 16.1$ and the positions to the ESO/SERC field nos. 351, 352, 411 and 412. In order to have profiles with better resolution and signal-to-noise ratio as well, galaxies with $13 < B_T < 14$ which fulfill selection criteria (i) and (iii) were chosen also.

The number of accurate redshifts available for galaxies in the magnitude range $13 < B_T < 16.1$ is small, so no selection according to redshift was made. For 11 of the selected galaxies, redshifts are found in the literature. It is planned to obtain redshifts for the other galaxies as well. The redshift information is important because the dust content of a spiral galaxy is closely connected to the luminosity; the brighter the galaxy, the more dust it contains.

For the galaxies with redshifts available, absolute B magnitudes were calculated using the apparent magnitudes given in Table 4 and a K-correction of $k = 3z$. A range of $-21.2 < M_B < -18.9$ with a mean of $< M_B >= -20.2$ is found. $H_0 = 70\,\mathrm{km\,s^{-1}\,Mpc^{-1}}$ and $q_0 = 0.5$ are adopted throughout this paper.

The galaxies were not explicitly chosen according to bulge-to-disc ratio. However, the bulge-to-disc ratio is implicitely given by the morphological type. Since galaxies with $2.0 \leq T \leq 4.0$ have significant bulges, the presence of the bulge must be taken into account. The selected galaxies were checked for dust lanes. No dust lanes were found.

Table 1 gives a list of the sample galaxies. The parameters are taken from the ESO-LV catalogue (Lauberts & Valentijn 1989). Apparent ellipticity ϵ and position angle PA are obtained from ellipse fits to B octants. PA is measured from north over east. Redshifts are given in Table 2.

Table 2. Redshift values for sample galaxies. Velocity cz is given in km/s

ESO-LV no.	cz	Reference
339−0120	5098	Huchra et al. (1995)
463−0200	2700	Bottinelli et al. (1990)
235−0080	5200	Sandage (1978)
286−0630	2668	Lawrence et al. (1994)
351−0180	5450	Lauberts & Valentijn (1989)
351−0250	10416	Maia et al. (1996)
351−0310	11605	Parker & Watson (1990)
412−0210	5514	Menzies et al. (1989)
352−0400	15130	Parker & Watson (1990)
352−0540	10421	Parker & Watson (1990)
352−0720	10563	Mathewson & Ford (1996)

2.2. Observations

The observations were carried out with the CCD camera of the 1.0 m telescope at the South African Astronomical Observatory (SAAO) in Sutherland, South Africa. The camera contains a Tek chip of 512×512 pixels. The pixel size is $27\,\mu$m which corresponds to a scale of 0.35 arcsec/pixel and to an image size of $3\farcm0 \times 3\farcm0$. The filters available are Johnson B and V and Cousins R and I.

The CCD images were obtained within 8 nights in September and October 1994. During 5.5 nights conditions were photometric, during the remaining 2.5 nights conditions were not photometric but still good enough for obtaining profiles with a reasonable signal-to-noise ratio. The seeing varied between $1\farcs2$ and $3\farcs0$ FWHM. ESO-LV 351−0180, 351−0220, 351−0240 and 351−0310 (B-image) are those galaxies which could only be observed in non-photometric conditions. The other galaxies were observed in photometric conditions.

For each CCD field B, V, R and I frames were taken. The exposure times were 900 s for each frame. For V, R and I, two frames were taken for each filter and for B four images were taken. This gives a total exposure time of 3600 s for B and 1800 s for V, R and I, respectively.

The CCD magnitudes are calibrated with the magnitudes of E-region stars given by Menzies et al. (1980). The magnitude and colour ranges of the chosen stars were $8.02 < V < 9.82$ and $0.11 < (B-V) < 1.61$, respectively. The standard stars were observed several times during a night with exposure times between 3 s and 40 s per frame. The data were used for determination of the transformation of the instrumental CCD magnitudes into the international $BVRI$ system.

2.3. Data reduction

Bias and flat field corrections as well as interpolations over bad pixels were done by SAAO staff. For each CCD frame the bias was measured from the overscan region. For flat field division mean flat fields were used. The accuracy of the corrected image is determined from the differences in the sky background in different areas of the CCD field after flat fielding. It is about 1%.

The dark current is negligible even for large integration times, so no dark correction was made. The long exposures show a number of cosmic ray events. These were removed from the images using the procedure described by Cunow (1993a). This method looks for "objects" with profiles which are steeper than those of the stars and replaces their pixels by the median of the surrounding area. The CCD images were checked for fringing. No fringing was found and no correction applied.

The final image for each galaxy and each filter was obtained by adding all frames for this galaxy and filter. The images were matched by using the positions of the stars. For each image the mode of an area undisturbed by stars was used for sky subtraction. Interactive checks of the background level assured that the correct sky value was subtracted. The uncertainty of the sky level due to gradients across the image area is about 0.3%. For a few galaxies, stars are found in front of the galaxy. These star pixels were flagged and neglected during the profile measurement. Surface brightness, ellipticity and position angle profiles were obtained by using the ellipse fitting procedure of the surface photometry package within MIDAS. The profiles were determined for each filter separately.

Photometric calibration was done with the standard star measurements. The instrumental magnitudes were corrected for extinction effects by applying the mean extinction coefficients obtained for this site (Menzies 1992). The standard star measurements were used for the determination of the magnitude zero points and the transformation of the instrumental CCD magnitudes into the international $BVRI$ system. The following transformation equations were applied:

$$B_{\rm CCD} = B + k_{1,B} + k_{2,B}X \quad (1)$$

$$V_{\rm CCD} = V + k_{1,V} + k_{2,V}X \quad (2)$$

$$R_{\rm CCD} = R + k_{1,R} + k_{2,R}X \quad (3)$$

$$I_{\rm CCD} = I + k_{1,I} + k_{2,I}X. \quad (4)$$

X is the airmass, $B_{\rm CCD}$, $V_{\rm CCD}$, $R_{\rm CCD}$ and are the instrumental magnitudes and B, V, R and I the magnitudes in the international system. For the standard stars, the comparison of the CCD magnitudes with the catalogue magnitudes shows a scatter of $\sigma = 0\fm06$ for B, $\sigma = 0\fm06$ for V, $\sigma = 0\fm06$ for R and $\sigma = 0\fm04$ for I. No colour term has been included in the transformation, because tests showed that no significant colour terms exist. According to these results, an accuracy of $0\fm06$ is expected for the surface brightness profiles of the galaxies. The surface photometry errors due to the uncertainties of flat field division and sky subtraction are obtained from the percentages determined above. They are given in Table 3.

Table 3. Errors of surface photometry due to flat fielding and sky subtraction errors determined for different surface brightness levels. μ and σ are given in mag arcsec^{-2}

$\mu(B)$	$\sigma(\mu(B))$	$\mu(V)$	$\sigma(\mu(V))$	$\mu(R)$	$\sigma(\mu(R))$	$\mu(I)$	$\sigma(\mu(I))$
23	0.04	22	0.03	21	0.01	21	0.02
24	0.12	23	0.06	22	0.03	22	0.04
25	0.40	24	0.19	23	0.06	23	0.12

3. Results

3.1. Integrated magnitudes

For each galaxy, total B, V, R and I magnitudes were measured from the CCD images. They were determined from apertures chosen interactively to assure that the diaphragm is large enough to contain the whole galaxy but still small enough to limit the magnitude error due to the sky error. Foreground stars within the aperture were removed interactively. Table 4 gives the magnitudes.

$B_{\rm T}$ and $R_{\rm T}$ obtained in this work were checked against the magnitudes given in the ESO-LV catalogue. It was found that the ESO-LV magnitudes are systematically brighter than those measured here. For the galaxies observed in photometric conditions, one obtains $< B_{\rm T} - B_{\rm T}({\rm ESO}) >= 0\overset{\rm m}{.}19 \pm 0\overset{\rm m}{.}06$ with a scatter of $\sigma = 0\overset{\rm m}{.}18$ and $< R_{\rm T} - R_{\rm T}({\rm ESO}) >= 0\overset{\rm m}{.}16 \pm 0\overset{\rm m}{.}04$ with a scatter of $\sigma = 0\overset{\rm m}{.}13$. These differences are in agreement with independent studies. Peletier et al. (1994) found that their B-magnitudes are $0\overset{\rm m}{.}23$, and their R-magnitudes $0\overset{\rm m}{.}12$ fainter than those in the ESO-LV catalogue. This result is difficult to interpret because the agreement of the magnitude differences indicate a systematic zero-point offset for the ESO-LV magnitudes. However, Paturel et al. (1994) compared $B_{\rm T}$ magnitudes in the ESO-LV catalogue with those given in the RC3 catalogue (de Vaucouleurs et al. 1991) and did not find any significant zero point differences between the two catalogues.

CCD magnitudes for the I-filter are available for ESO-LV 463−0200, 351−0180, 351−0250, 412−0210 and 352−0720 (Mathewson & Ford 1996). Comparison with total I-magnitudes obtained in this work for the galaxies observed in photometric conditions gives a mean difference of $< I_{\rm T} - I_{\rm T}({\rm MF}) >= 0\overset{\rm m}{.}15 \pm 0\overset{\rm m}{.}03$ with a scatter of $0\overset{\rm m}{.}05$. This shows that there exists a zero-point difference between the two magnitude systems with the magnitudes obtained in this work being systematically fainter. The reason for this difference could not be found.

For the galaxies observed in non-photometric conditions, comparison of $B_{\rm T}$ and $R_{\rm T}$ with the ESO-LV data and of $I_{\rm T}$ with the data of Mathewson & Ford does not show any significant deviations from the magnitude differences obtained for the galaxies measured in photometric conditions. This indicates that for these galaxies the errors for integrated magnitudes and surface brightness due to the weather conditions can be regarded as smaller than $0\overset{\rm m}{.}1$.

Table 4. Total magnitudes $B_{\rm T}$, $V_{\rm T}$, $R_{\rm T}$ and $I_{\rm T}$ and apparent ellipticity ϵ and position angle PA for the sample galaxies. ϵ and PA are obtained from the surface brightness profiles in R and are given for $\mu(R) = 21.5$ mag arcsec^{-2}

ESO-LV	$B_{\rm T}$	$V_{\rm T}$	$R_{\rm T}$	$I_{\rm T}$	ϵ	PA(°)
339−0120	14.06	13.32	12.79	12.29	0.36	3.4
463−0200	13.47	13.19	12.32	11.94	0.63	158.2
235−0080	13.28	12.74	12.28	11.73	0.25	131.3
286−0630	14.04	13.44	12.99	12.49	0.48	46.1
411−0170	15.74	14.77	14.23	13.62	0.51	69.7
351−0180	15.39	14.84	14.31	13.91	0.65	-3.4
351−0220	15.42	14.68	14.39	13.96	0.46	162.7
351−0240	16.19	15.28	14.82	14.05	0.61	142.7
351−0250	15.30	14.57	14.09	13.49	0.28	126.0
351−0310	15.49	14.67	14.18	13.59	0.33	166.7
412−0210	15.39	14.49	13.89	13.27	0.62	38.6
352−0400	15.66	14.87	14.45	13.83	0.52	187.5
352−0540	15.33	14.45	13.88	13.22	0.83	126.1
352−0720	15.54	14.65	14.07	13.35	0.79	173.5

3.2. Profiles

Figure 1 shows surface brightness μ, apparent ellipticity ϵ and position angle PA plotted against the apparent semi-major axis r for the sample galaxies. ϵ and PA are plotted for the R-filter because the R-images are those with the highest signal-to-noise ratio and the ellipticity as well as the position angle profiles are very similar for different wavelength regions.

For galaxies which are not edge-on, the inner parts of the profiles are dominated by the light distribution of the bulge while the outer parts are dominated by the spiral arms. For galaxies with prominent spiral arms (ESO-LV 339−0120, 235−0080 and 352−0400), apparent ellipticity and position angle vary strongly throughout the galaxy.

For edge-on or nearly edge-on galaxies (ESO-LV 463−0200, 351−0240, 352−0540 and 352−0720), the inner parts of the profiles are dominated by the bulge, while the outer parts are dominated by the overall shape of the disc. The apparent ellipticity is small in the center, but

Table 5. Parameters for exponential disc. Scalelengths r_D are measured along the semimajor axis and are given in arcsec; central surface brightnesses μ_D are given in mag/arcsec^2. "Range" gives the range of the semimajor axis in arcsec used for the fit

ESO-LV no.	$r_D(B)$	$r_D(V)$	$r_D(R)$	$r_D(I)$	$\mu_D(B)$	$\mu_D(V)$	$\mu_D(R)$	$\mu_D(I)$	Range
339−0120	23.8	21.4	21.2	20.7	21.75	20.92	20.36	19.83	7–24
463−0200	22.1	19.2	18.6	16.9	20.83	20.36	19.43	18.91	10–49
235−0080	6.4	7.3	7.5	7.9	19.04	18.85	18.50	18.13	16–26
286−0630	–	7.2	7.2	7.1	–	18.61	18.16	17.66	17–31
411−0170	7.2	5.7	5.3	5.1	21.88	20.52	19.82	19.16	7–12
351−0180	12.8	11.0	10.5	8.4	21.77	20.96	20.29	19.62	10–24
351−0220	6.8	6.8	6.4	6.1	21.02	20.29	19.83	19.38	7–21
351−0240	18.2	13.8	12.7	11.3	22.51	21.34	20.71	19.86	9–21
351−0250	6.5	7.0	6.9	6.9	21.04	20.52	20.02	19.49	9–21
351−0310	6.5	5.7	5.7	5.4	21.05	20.01	19.53	18.87	12–19
412−0210	7.8	7.8	7.5	6.8	21.06	20.25	19.59	18.85	10–31
352−0400	–	4.0	3.8	3.8	–	19.79	18.87	18.28	10–17
352−0540	24.5	18.4	16.0	13.9	21.89	20.72	19.84	19.05	10–31
352−0720	19.3	15.8	15.0	11.1	21.96	20.86	20.21	19.16	9–21

throughout the linear part of the surface brightness profile, ϵ increases systematically until it reaches a constant value, which is the true apparent ellipticity of the galaxy disc.

For each galaxy, ϵ and PA for $\mu = 21.5\,\mathrm{mag\,arcsec^{-2}}$ in the R-filter are taken as a measure for ϵ and PA of the whole galaxy. This isophote has been chosen because it is well within the disc. Table 4 gives magnitudes, apparent ellipticity and position angle for each galaxy. Comparison with the values given in the ESO-LV catalogue shows a good agreement for almost all sample galaxies. The mean differences are $<\epsilon-\epsilon(\mathrm{ESO})>=0.04\pm0.04$ with a scatter of 0.14 and $<\mathrm{PA}-\mathrm{PA(ESO)}>=3.9^\circ\pm1.9^\circ$ with a scatter of 7.3°. There is, however, one galaxy for which the ϵ-value given in the ESO-LV catalogue strongly deviates from that obtained from the profile. This is found for ESO-LV 352−0720, where $\epsilon = 0.39$ is given in the ESO-LV catalogue. The galaxy image shows an object with very high ellipticity, so the value of 0.39 is not representative for the outer parts of this galaxy. The value of $\epsilon = 0.79$ found in this work is much more realistic for the galaxy as a whole.

The surface brightness profiles obtained in photometric conditions were compared to those given in the literature. The ESO-LV catalogue contains low-resolution photographic surface brightness profiles in B and R for all sample galaxies. For B, a mean difference of $<\mu(B)-\mu(B)(\mathrm{ESO})>=0.16\pm0.07\,\mathrm{mag\,arcsec^{-2}}$ with a scatter of $\sigma=0.40\,\mathrm{mag\,arcsec^{-2}}$ was found. For R, the mean difference is $<\mu(R)-\mu(R)(\mathrm{ESO})>=0.18\pm0.07\,\mathrm{mag\,arcsec^{-2}}$ with a scatter of $\sigma=0.42\,\mathrm{mag\,arcsec^{-2}}$. The profiles obtained in this work are systematically fainter than the ESO-LV profiles. Most of this deviation is explained by the magnitude zero-point difference. Part of the deviation is found in the outer parts of the profiles, i.e. the profiles obtained in this work are steeper than those in the ESO-LV catalogue. It is not clear what causes this deviation. The differences are probably not due to the uncertainty in the sky subtraction. As a check the images with the fitted ellipses were subtracted from the original image. For none of the sample galaxies, any significant parts of the galaxies are found to be remaining after subtraction.

I-profiles of four of the sample galaxies observed in photometric conditions (ESO-LV 463−0200, 351−0250, 412−0210 and 352−0720) are also found in Mathewson & Ford (1996). The mean surface brightness difference is $<\mu(I)-\mu(I)(\mathrm{MF})>=0.26\pm0.04\,\mathrm{mag\,arcsec^{-2}}$ with a scatter of $\sigma=0.16\,\mathrm{mag\,arcsec^{-2}}$. As for the B and R filters, this is larger than expected from the magnitude zero-point difference, but is in a better agreement than the $\mu(B)$- and $\mu(R)$-profiles with the ESO-LV catalogue.

3.3. Disc scalelengths

In order to determine scalelength r_D and central surface brightness μ_D of the disc, an exponential law was fitted to the surface brightness profiles of each sample galaxy. Since the linear parts of the profiles are the ones dominated by the disc, these parts were used for the fit. Bulge parameters were not fitted because the angular diameters of the bulges are so small that they are strongly influenced by seeing.

Table 5 shows the results obtained for r_D and μ_D. The $\mu(B)$-profiles for ESO-LV 286−0630 and ESO-LV 352−0400 do not show any linear parts, so no fits were made for them. In order to obtain a scalelength which is not influenced by the inclination angle of the galaxy, r_D is measured along the apparent semimajor axis. The errors for r_D and μ_D are obtained by comparing the values for different sub-parts of the linear parts of the profiles. ESO-LV 463−0200 and 351−0180 could be observed twice.

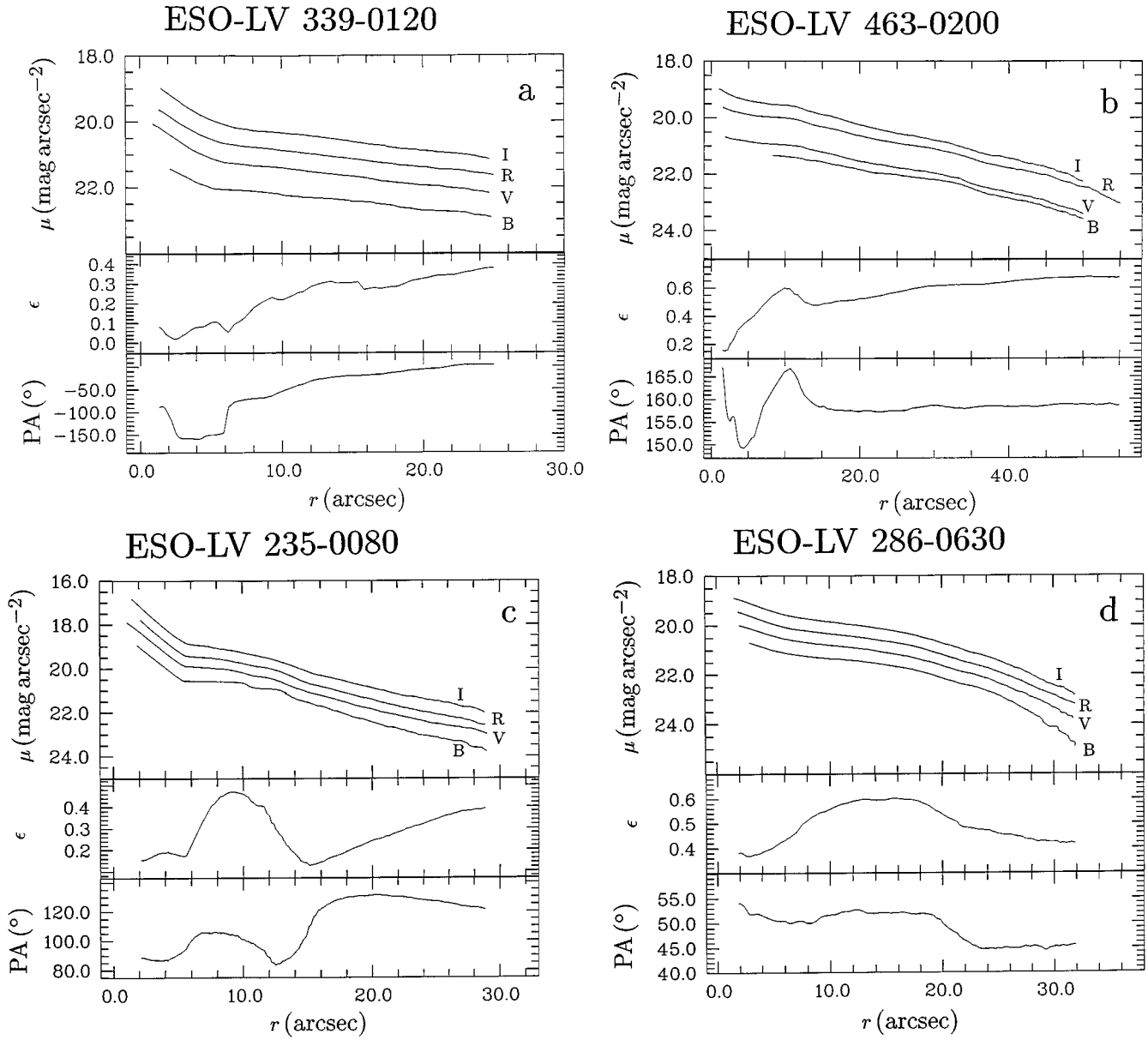

Fig. 1. Surface brightness μ, apparent ellipticity ϵ and position angle PA against semimajor axis r. ϵ and PA are taken from the R images. For details see text

The sets of images were taken under different seeing conditions. The difference of $\mu_{\rm D}$ and $r_{\rm D}$ found between these two sets are also used to determine the error. The errors obtained for $r_{\rm D}$ and $\mu_{\rm D}$ are similar for each galaxy and filter. Typical values are $\sigma(r_{\rm D}) = 10\%$ and $\sigma(\mu_{\rm D}) = 0\overset{\rm m}{.}1$.

It has been found by many authors that the surface brightness profiles of spiral galaxies often show deviations from an exponential law, which sometimes makes the definition of the linear part difficult. As can be seen in Fig. 1, such deviations are present in the galaxies studied here. The error of 10% for $r_{\rm D}$ is mainly due to these deviations.

The selection of the profile parts used for the fit was checked with the $B-I$ and $V-I$ colour profiles. For an exponential disc, colour profiles are linear. So the chosen parts should be those for which the colour profiles show least deviation from linearity, which was confirmed for the present sample.

For the 11 sample galaxies for which redshifts are available (see Table 2), disc scalelengths were determined in kpc. The mean values are: $< r_{\rm D}(B) >= 6.8 \pm 1.6$ kpc, $< r_{\rm D}(V) >= 5.3 \pm 1.1$ kpc, $< r_{\rm D}(R) >= 5.0 \pm 1.0$ kpc and $< r_{\rm D}(I) >= 4.5 \pm 0.8$ kpc. These results are in agreement with values found for other samples of spiral galaxies (e.g., Kent 1985; van der Kruit 1987; Andredakis & Sanders 1994; Courteau 1996).

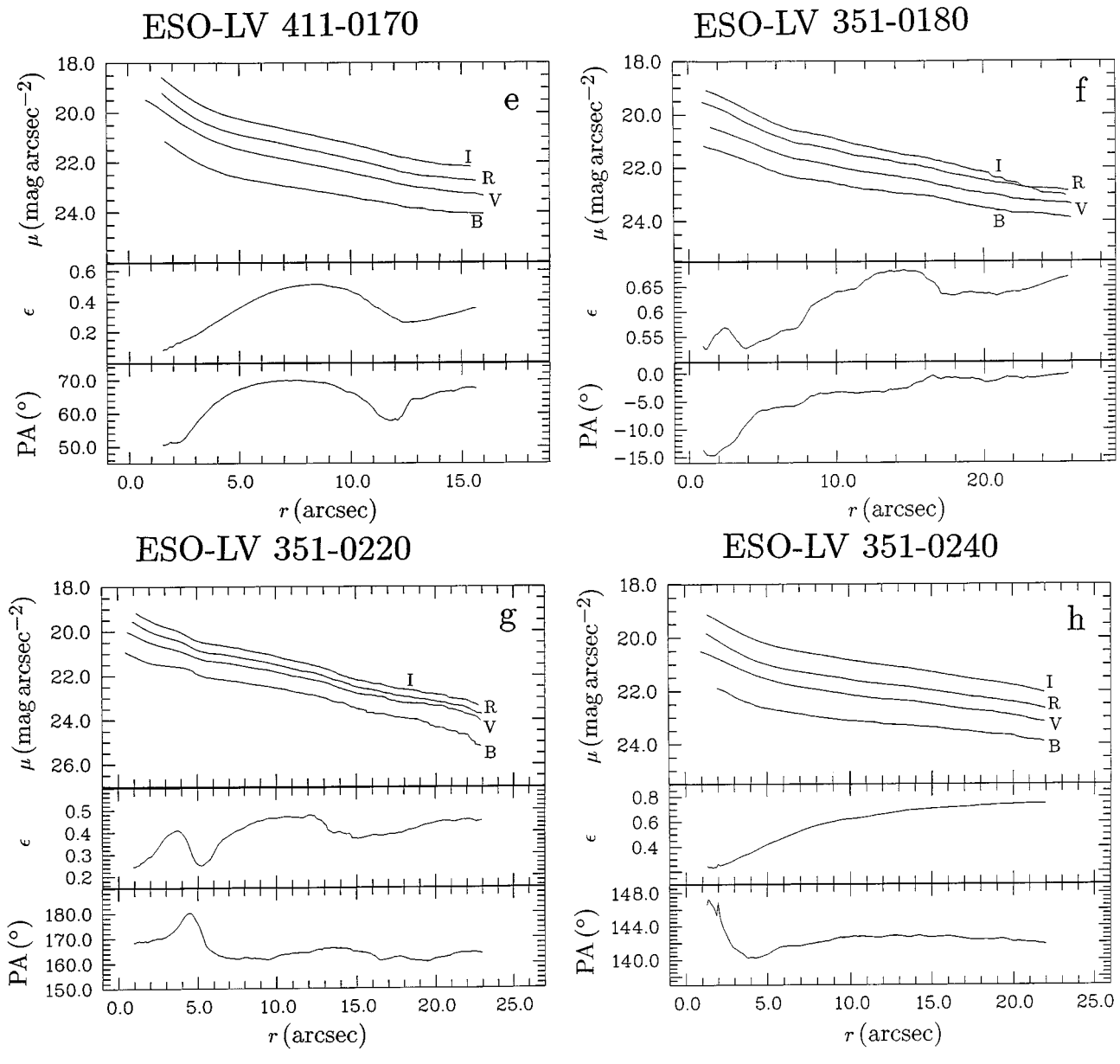

Fig. 1. continued

For 13 of the 14 sample galaxies, the disc scalelength decreases systematically with increasing wavelength. ESO-LV 235−0080 shows the opposite behaviour, the disc scalelength increases systematically with increasing wavelength. For ESO-LV 351−0250, disc scalelengths increase slightly from I to V, but $r_{\rm D}(B)$ is deviating. ESO-LV 351−0250 is the only galaxy in the present sample for which an active nucleus was found. Maia et al. (1996) detected [OIII] emission at a rest wavelength $\lambda = 5007$ Å. It is not clear yet if the surface brightness profiles of active galaxies show systematic differences compared to those of normal galaxies. Table 6 gives the mean scalelength ratios and their scatter for the different colours.

Table 6. Mean values and scatter for disk scalelength ratios

Ratio	mean	scatter
$< r_{\rm D}(B)/r_{\rm D}(I) >$	1.31	0.29
$< r_{\rm D}(V)/r_{\rm D}(I) >$	1.14	0.14
$< r_{\rm D}(R)/r_{\rm D}(I) >$	1.13	0.20

The systematic increase of disc scalelengths with decreasing wavelength has already been found by various authors. Elmegreen & Elmegreen (1984) obtained $< r_{\rm D}(B)/r_{\rm D}(I) >= 1.16$ for face-on galaxies. The value found in this work is larger, which is due to the fact

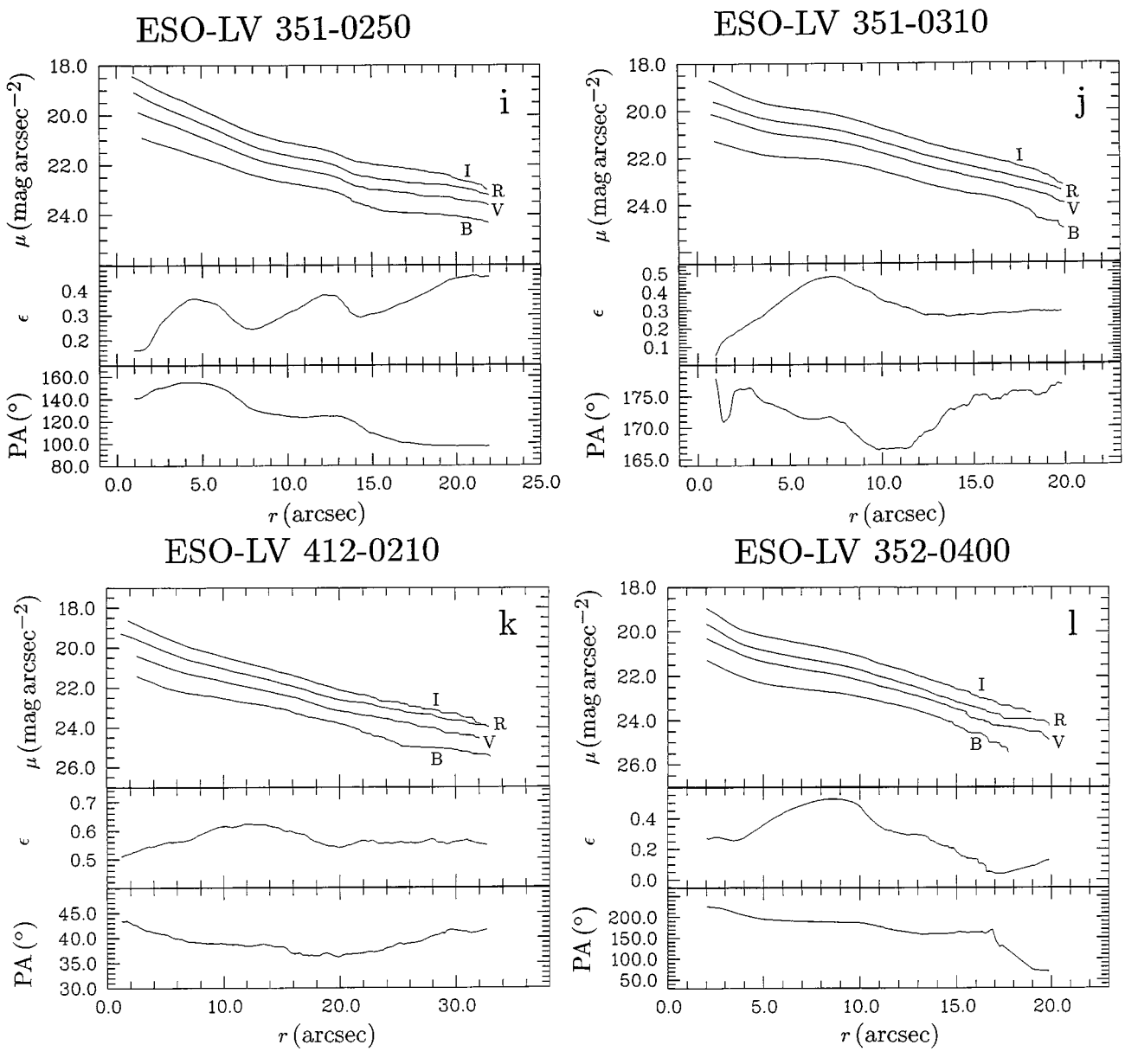

Fig. 1. continued

that the present sample does not include face-on galaxies only but also galaxies with larger inclination angles, which show larger ratios (see below).

Peletier et al. (1994) found that for bright galaxies with $M_K < -22$ the ratio of the disc scalelengths in B and K, $r_D(B)/r_D(K)$, increases systematically with increasing apparent ellipticity. Figure 2 shows disk scalelength ratios $r_D(B)/r_D(I)$, $r_D(V)/r_D(I)$ and $r_D(R)/r_D(I)$ for the present sample. The trend found by Peletier et al. for $r_D(B)/r_D(K)$ is found for the optical and near infrared wavelength regions as well. The larger the difference in wavelength between the two bands, the larger is the increase of the scalelength ratio with increasing apparent ellipticity. These results confirm that significant colour gradients are present in the discs of the sample galaxies and that these gradients are larger for larger inclination angles.

Byun et al. (1994) simulated galaxy images for different amounts of dust, determined disc scalelengths and calculated scalelength ratios $r_D(B)/r_D(I)$ (see their Fig. 10). Unlike the galaxies investigated in this work, the model galaxies presented in Fig. 10 do not have bulges. For central face-on optical depths in the V-band, $\tau_v(0) = 0.5, 1, 2$, the simulated ratios increase systematically with increasing inclination angle by $\leq 10\%$. For larger amounts of dust, $\tau_v(0) = 5, 10$, the ratio is constant or decreases slightly.

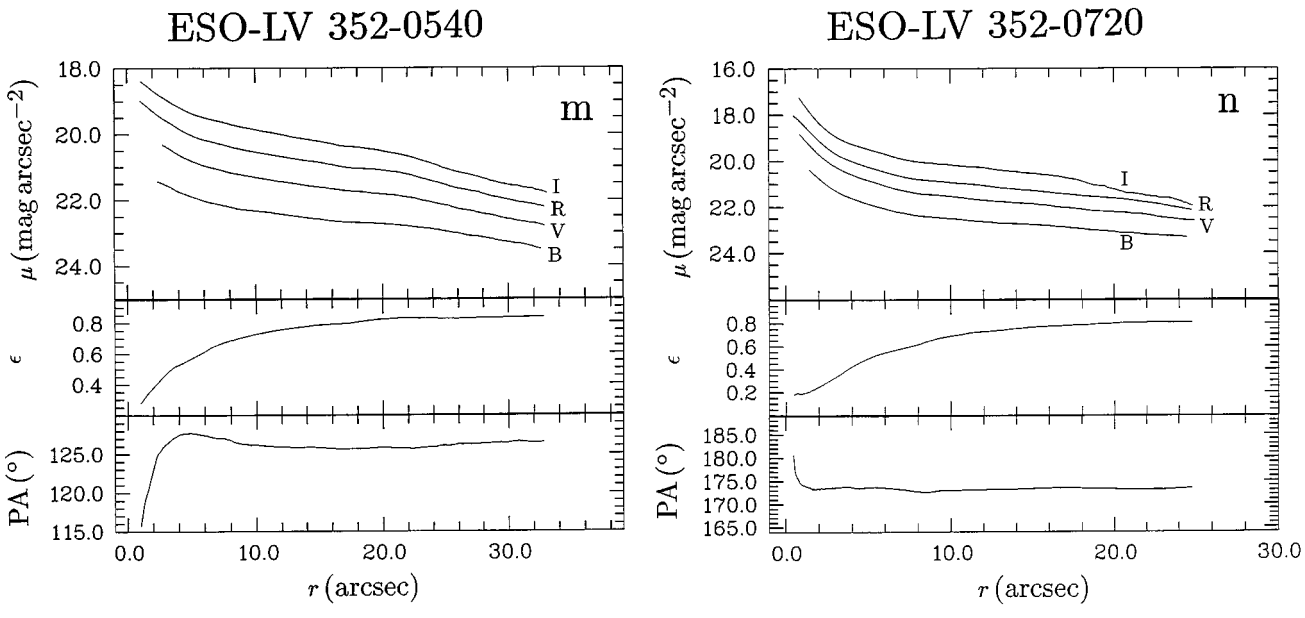

Fig. 1. continued

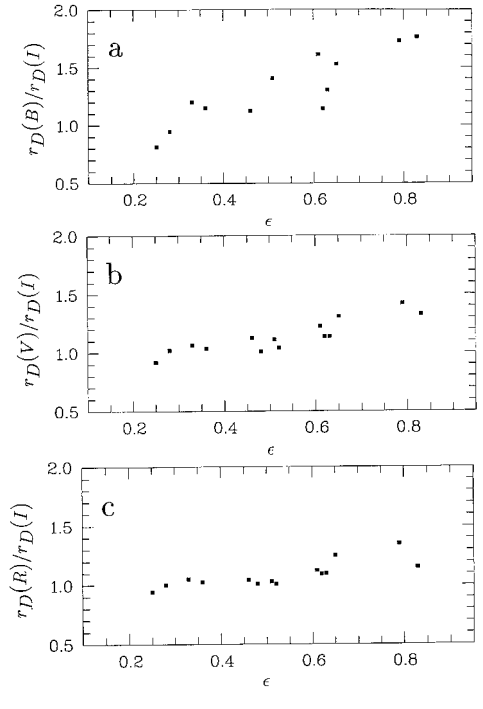

Fig. 2. Disc scalelength ratios plotted against apparent ellipticity ϵ measured in the R-filter at $\mu = 21.5\,\mathrm{mag\,arcsec^{-2}}$. **a)** shows the scalelength ratios between B and I, **b)** shows the ratios between V and I and **c)** between R and I

This result is not in agreement with the ratios measured in this work (see Fig. 2a). For edge-on galaxies, $r_\mathrm{D}(B)/r_\mathrm{D}(I)$ is about 80% larger than for face-on galaxies. Byun et al. obtained their scalelengths from major-axis radial profiles, while in this work scalelengths are measured from elliptically-averaged profiles. Byun et al. stress that for galaxies with a significant large differences exist between the two types of profiles, especially for highly inclined objects. In the present work however, the fitting ranges for the scalelength measurements are chosen to be in the outer parts of the galaxy where the influence of the bulge is small, so the observed scalelengths should not be significantly affected. Furthermore, even if one excludes the highly inclined galaxies (e.g., objects with $\epsilon > 0.6$), Fig. 2a is still not in agreement with any of the model curves. So even though the comparison is difficult, evidence remains that the present data show a larger increase of scalelength ratio with increasing inclination than is predicted by Byun et al. (1994).

Before any final conclusions can be drawn the following steps are necessary: (i) the number of sample galaxies must be enlarged, (ii) for model galaxies with a bulge, scalelength ratios must be calculated from elliptically-averaged profiles, and (iii) the possibility of intrinsic colour gradients within the stellar disc due to population gradients must be taken into account. It is planned to simulate galaxy images with a wider variety of parameters than those used by Byun et al. in order to see if the observed results can be reproduced.

Acknowledgements. I would like to thank Dr. R.S. Stobie for allocation of observing time at SAAO/Sutherland. It is a pleasure to thank Drs. J.W. Menzies and J. Caldwell for assistance during the observations, Mrs. I. Bassett for prereducing the CCD images, and Profs. W.F. Wargau and W. Seitter for many useful discussions concerning galaxies and their properties. Special thanks go to the referee, Dr. F. Simien, for important and helpful comments, and to Dr. R. Dümmler for carefully reading the manuscript. Financial support of this

work by the Deutsche Forschungsgemeinschaft DFG under the number Se 345/22-1 and by the Ministerium für Wissenschaft und Forschung des Landes Nordrhein-Westfalen/Germany (Lise-Meitner-Stipendium) is gratefully acknowledged. Finally, I thank ESO for the use of the MIDAS software for the calculation of the surface brightness profiles. This research has made use of the Simbad database at CDS, Strasbourg, France, and of the Lyon-Meudon Extragalactic Database (LEDA) supplied by the LEDA team at the Observatoire de Lyon.

References

Andredakis Y.C., Sanders R.H., 1994, MNRAS 267, 283
Block D.L., Bertin G., Stockton A., Grosbøl P., Moorwood A.F.M., Peletier R.F., 1994a, A&A 288, 365
Block D.L., Witt A.N., Grosbøl P., Stockton A., Moneti A., 1994b, A&A 288, 383
Bottinelli L., Gougenheim L., Fouqué P., Paturel G., 1990, A&AS 82, 391
Byun Y.I., Freeman K.C., Kylafis N.D., 1994, ApJ 432, 114
Courteau S., 1996, ApJS 103, 363
Cunow B., 1992, MNRAS 258, 251
Cunow B., 1993a, A&AS 97, 541
Cunow B., Wargau W.F., 1996, New Extragalactic Perspectives in the New South Africa, Block D.L. and Greenberg J.M (eds.). Kluwer, Dordrecht, p. 353
de Vaucouleurs G., de Vaucouleurs A., Corwin H.G.Jr., Buta R.J., Paturel G., Fouqué P., 1991, Third Reference Catalogue of Bright Galaxies. Springer New York
Elmegreen D.M., Elmegreen B.G., 1984, ApJS 54, 127
Evans R., 1994, MNRAS 266, 511
Héraudeau Ph., Simien F., Mamon G.A., 1996, A&AS 117, 417
Héraudeau Ph., Simien F., 1996, A&AS 118, 111
Huchra J.P., Geller M.J., Clemens C.M., Tokarz S.P., Michel A., 1995, The CFA redshift catalogue, Harvard Smithsonian Center for Astrophysics, Harvard
Kent S.M., 1985, ApJS 59, 115
Lauberts A., Valentijn E.A., 1989, The Surface Photometry Catalogue of the ESO-Uppsala Galaxies, European Southern Observatory (ESO-LV catalogue)
Lawrence A., et al., 1994, MNRAS, Preprint (citation from LEDA database)
Maia M.A.G., Suzuki J.A., da Costa L.N., Willmer C.N.A., Rité C., 1996, A&AS 117, 487
Mathewson D.S., Ford V.L., 1996, ApJS 207, 97
Menzies J.W., 1992 (private communication)
Menzies J.W., Banfield R.M., Laing J.D., 1980, Circ. S. Afr. Astron. Obs. 1, 149
Menzies J.W., Coulson I.M., Sargent W.L.W., 1989, AJ 97, 1576
Parker Q.A., Watson F.G., 1990, A&AS 84, 455
Paturel G., Bottinelli L., Gouguenheim L., 1994, A&A 286, 768
Peletier R.F., Valentijn E.A., Moorwood A.F.M., Freudling W., 1994, A&AS 108, 621
Sandage A., 1978, AJ 83, 904
Schuecker P., Ott H.-A., Seitter W.C., 1996a, ApJ 472, 485
Schuecker P., Ott H.-A., Seitter W.C., 1996b, ApJ 459, 467
van der Kruit P.C., 1987, A&A 173, 59